AN EQUIVALENT CIRCUIT FOR SMALL

ATRIAL TRABECULAE OF FROG

E. JAKOBSSON, L. BARR, *and* J. A. CONNOR

From the Department of Physiology and Biophysics, University of Illinois, Urbana, Illinois 61801

ABSTRACT   An equivalent electrical circuit has been constructed for small atrial trabecula of frog in a double sucrose gap voltage clamp apparatus.   The basic strategy in constructing the circuit was to derive the distribution of membrane capacitance and extracellular resistance from the preparation's response to small voltage displacements near the resting condition, when the membrane conductance is presumably quite low.   Then standard Hodgkin-Huxley channels were placed in parallel with the capacitance and the results of voltage clamp experiments were simulated.   The results suggest that the membranes of the preparation cannot in fact be clamped near the control voltage nor can the ionic currents be measured directly with reasonable accuracy by axon standards.   It may or may not be a realizable goal in the future to define the preparation's electrical behavior well enough to permit the ultimate quantitative description of the membrane's specific ion conductances.   The results of this paper suggest that if this goal is achieved using the double sucrose gap voltage clamp, it will be by a detailed quantitative accounting for substantial irreducible errors in voltage control, rather than by experimental achievement of good voltage control.

INTRODUCTION

Voltage clamping of excitable membranes has been done successfully for over 20 years (Hodgkin and Huxley, 1952 *a-c*).   The great advantage of such experiments for the theoretical analysis of ion movement across membranes lies in the almost pure dependence of the kinetics of ion permeability changes on membrane voltage (Hodgkin and Huxley, 1952 *d*).   After the initial work on squid, there followed successful extensions to other single cell preparations (Cole, 1968).   Extensions of the technique to cardiac muscle involve new considerations because the cells of this tissue are so small and well connected that clamp experiments on single cells have not been possible.   Some workers before us have reported current and voltage traces similar to those for axons when applying the double sucrose gap voltage clamp technique to strips of frog cardiac muscle (Rougier et al., 1968; Tarr, 1971).   However, others have pointed out ways in which such results might be artifactual, and have asserted that serious problems of membrane voltage control might be present simultaneously with apparently good voltage clamp records (Johnson and Lieberman, 1971; Tarr and Trank, 1974).   We have made an experimental (Connor et al., 1975) and theoretical investigation into this situation for small atrial trabeculae ($< 100 \mu$m diameter) of frog in the double sucrose gap

voltage clamp. The theoretical investigation has been aimed at constructing an equivalent circuit appropriate for this tissue in our experimental apparatus. Our fundamental strategy in constructing such a circuit has been to deduce the distribution of membrane capacitance and extramembrane resistance from morphological considerations and from the measured behavior of the preparation in response to small voltage disturbances near the resting condition (a condition in which the membrane resistance is relatively high). Then Hodgkin-Huxley sodium conductance channels were added in parallel to the membrane capacitance elements and the computed behavior of the resulting equivalent circuit was compared with the measured behavior of the actual preparation. The results of the comparison are detailed in this paper. These results are not directly applicable to other heart muscle preparations and other voltage clamp techniques, but the extra-membrane resistance which we find so important is probably important in those cases too. Some work has been done by others with other preparations toward constructing equivalent circuits related to structure and exploring their electrical behavior by computer simulation. Especially notable is work in cardiac Purkinje fibers (Hellam and Studt, 1974 a, b) and skeletal muscle (Adrian and Peachey, 1973).

METHODS

Our basic experimental method is the double sucrose gap, with the boundaries between the saline test node and the insulating sucrose cuffs established by the flow patterns of the sucrose and saline solutions. Our preparations are frog atrial trabeculae with an outer diameter of 40–80 μm. All data and computer simulations, unless otherwise specifically stated, refer to a test node width of 100 μm. More detailed experimental methods are given in our previous paper (Connor et al., 1975). Numerical solutions of differential equations were obtained on the University of Illinois IBM 360-75 using the Continuous Systems Modeling Program, which provides for a choice of numerical integration methods. The method used for the computations presented in this paper was fourth-order Runge-Kutta with variable integration interval.

THEORY AND RESULTS

The response of an R-C network to a step perturbation is determined by the distribution of resistances and capacitances. When a small voltage step is placed on one of our trabeculae with the test node width at our normal 100 μm, the resulting decay of capacitive current normally requires three time constants, or a sum three terms decaying exponentially in time, to be simulated accurately (Connor et al., 1975). The presence of three time constants means that an accurate equivalent circuit for the preparation can have no fewer than three capacitors. It may have more than three, but three is minimal. The next step in constructing the equivalent circuit is to decide how to connect the three or more capacitors with resistors; the key resistances will be those across which the highest voltage difference obtains during voltage clamp. Examination of electron micrographs of this tissue shows the extracellular pathways for current flow to be tortuous and narrow, while the interiors of the cells look better connected elec-

trically to each other (provided one assumes the nexuses to be low-resistance pathways). A quantitative reason for believing the intracellular resistance to be relatively low is given by dividing the measured values of high frequency input resistance at the voltage pool by the length of tissue bathed by the sucrose collar (Connor et al., 1975). This method gives a figure for resistivity of the intracellular medium of 200–400 Ω-cm, comparable to what one would expect if the intracellular volume of the trabecula were a single freely diffusible saline medium.

If we assume that the resistances which are the primary determinants of the preparation's behavior in the test node are extracellular, the next question is whether the large voltage gradients through these resistances are longitudinal (along the length of the preparation) or radial (perpendicular to the length of the preparation). An answer to this question is suggested in the resistance of the preparation to ringing, or oscillations (our previous paper, Connor et al., 1975). For our normal amplifier bandwidth of 0–50 kHz, the node width on our preparations can be increased to the range of 300–400 μm before oscillations become evident. Given that the membrane area/cross-section area ratio for these preparations is appropriate for cells about 5 μm in diameter, we would expect in the absence of a strong resistance to extracellular current flow in the radial direction that such cells would oscillate at a much smaller node width. Thus, we conclude that these preparations exhibit a large extracellular resistance to current flow in the radial direction and, consequently, large voltage drops along that resistance when current is injected into the preparation. Connor et al., 1975, show the results of passive cable simulations in which the resistance to radial current flow is varied but the other cable parameters are held at values appropriate for one of our trabeculae. It is seen that the simulation with high radial resistance has oscillatory characteristics much closer to the biological preparations. We know, of course, that there will in fact be significant voltage drop in the longitudinal direction within the test node. Thus, we know in advance that the equivalent circuit derived from the above considerations will be to some extent imperfect, but it will be the simplest reasonable equivalent circuit to use to begin to explore the effects of certain conditions we know must exist within the tissue (i.e. distributed capacitive elements separated by high resistances).

We thus have chosen as our working hypothesis that the major resistive determinant of the test node R-C response to small voltage steps is extracellular resistance to *radial* current flow. This, together with the R-C response itself and together with the morphology of the tissue, is sufficient to define the equivalent R-C passive circuit as that shown in Fig. 1. (Leak conductance is left out of Fig. 1 and the derivation of Eqs. 2–7 for simplicity in algebra. Computer simulations of the capacitive response in which 0.1 mmhos/cm^2 leak was inserted show that this approximation gives only a small error.) Our assumption about our voltage clamp experiments vis-à-vis this equivalent circuit is that we can achieve good voltage control between the bathing solution and the cell interiors in the test node. Clearly this will not be exactly equivalent to good voltage control across the membrane capacitance (C_{m0}, C_{m1}, and C_{m2}).

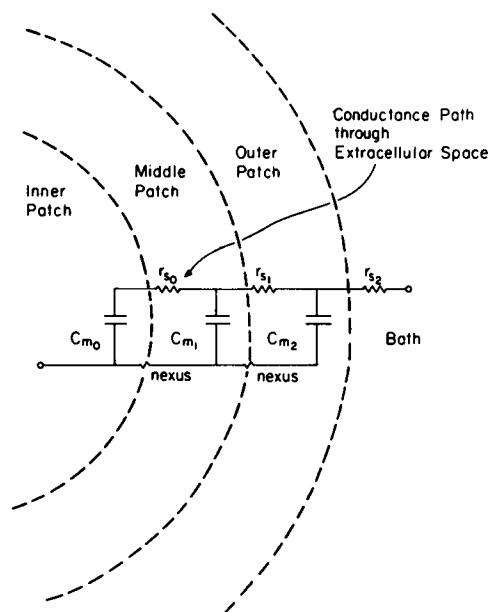The capacitive transient current for a small voltage step change, ΔV, on our prepara-

FIGURE 1 Distribution in trabecular cross section of extracellular resistances and capacitances consistent with measured capacitive transients (ionic conductance channels omitted).

tion is well fit by the expression:

$$(I - I_l)/\Delta V = Ae^{-t/\tau_a} + Be^{-b/\tau_b} + Ce^{-c/\tau_c}. \tag{1}$$

If we assume that our measured ΔV is equal to the voltage difference between the cell interiors and the bathing solution, and if we further assume that the membrane conductance for small steps near the resting condition is low, then expressions for $r_{s0}, r_{s1}, r_{s2}, C_{m0}, C_{m1}$, and C_{m2} in terms of A, a, B, b, C, c are (after some algebra) as follows:

$$r_{s2} = \Sigma^{-1}, \tag{2}$$

$$C_{m2} = (r_{s2}^2 \Sigma')^{-1}, \tag{3}$$

$$r_{s1} = [(\Sigma'' C_{m2}/\Sigma') - (1/r_{s2})]^{-1}, \tag{4}$$

$$C_{m1} = \Sigma'/(r_{s1}[r_{s1}\Sigma''' C_{m2} - \Sigma''(1 + r_{s1}/r_{s2})]), \tag{5}$$

$$C_{m0} = \Sigma' - C_{m1} - C_{m2}, \tag{6}$$

$$r_{s0} = (1/C_{m1} + 1/C_{m0})/[(1/\tau_a + 1/\tau_b + 1/\tau_c)$$
$$- (1/r_{s1} + 1/r_{s2})/C_{m2} - (C_{m1}r_{s1})^{-1}], \tag{7}$$

where

$$\Sigma \equiv A + B + C,$$

$$\Sigma' \equiv A/\tau_a + B/\tau_b + C/\tau_c,$$

$$\Sigma'' \equiv A/\tau_a^2 + B/\tau_b^2 + C/\tau_c^2,$$

$$\Sigma''' \equiv A/\tau_a^3 + B/\tau_b^3 + C/\tau_c^3.$$

It will be noted that Eqs. 2–7 must be applied in order, since each uses the result obtained in the previous one.

Values of r_{s0}, r_{s1}, r_{s2}, C_{m0}, C_{m1}, C_{m2} calculated from Eqs. 2–7 for some of our preparations are given in Table I. At first glance the series resistance we have measured and used in computations may appear so large as to make this preparation atypical. Indeed, values of total R_s in our experiments ranged between 20 and 100 KΩ whereas values more on the order of 500 Ω are reported for mammalian preparations (Beeler and Reuter, 1970). The discrepancy is more a matter of total preparation size though than any fundamental difference in the tissues. If total series resistance is converted to a per unit area (estimated) basis, the figure for our preparations averages approximately 0.18 KΩ normalized to 1 cm^2 of membrane area. This compares favorably with the estimate for mammalian trabecula of 500 Ω for 1 cm^2 made by Kootsey and Johnson (1972) from the data of Beeler and Reuter (1970). Therefore the considerations brought about by series resistance that we have described here cannot necessarily be ignored in other preparations.

We should note that we have no evidence that the preparations are in fact composed of three discrete segments of tissue. Indeed, it seems rather more likely that the capacitive transient decays with a continuous spectrum of relaxation times. Eigen and DeMaeyer (1963) point out that a continuous relaxation spectrum is typical of diffusion-controlled processes, and also that individual components of a relaxation

TABLE I

TYPICAL VALUES OF r_{s0}, r_{s1}, r_{s2}, C_{m0}, C_{m1}, C_{m2} IN OUR EQUIVALENT CIRCUIT, CALCULATED FROM EXPERIMENTAL DATA BY USE OF EQS. 2–7

| Prep. no.	Node width	Diam	R_{s2}	C_{m2}	R_{s1}	C_{m1}	R_{s0}	C_{m0}
	µm	µm	kΩ	µF	kΩ	µF	kΩ	µF
6273	60	75	79.4	0.00517	107.1	0.00442	491.6	0.00294
6273	100	75	42.9	0.00881	144.2	0.00560	710.3	0.00895
6274	60	60	37.3	0.00347	75.3	0.00235	640.7	0.00232
6274	100	60	44.1	0.00367	226.7	0.00301	1242.4	0.00185
6274	150	60	35.5	0.00500	257.3	0.00097	845.5	0.00520
6272	50	60	46.6	0.00344	175.5	0.00332	1271.4	0.00427
6272	100	60	35.7	0.00646	437.0	0.00307	944.7	0.00667
7241	66	66	93.5	0.00371	146.2	0.00371	667.7	0.00560
7241	100	66	58.4	0.00691	334.3	0.00496	747.9	0.00485
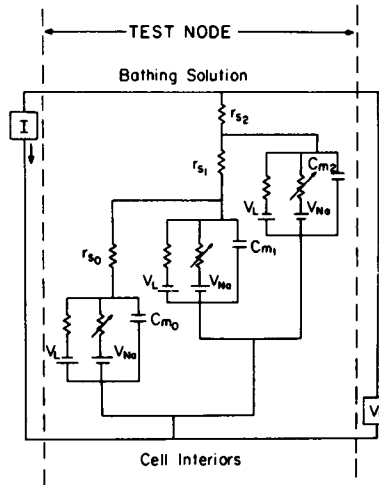
FIGURE 2 Electrical equivalent circuit for frog atrial trabecula in test node of double sucrose gap.

spectrum have to differ by several-fold to be resolvable by the type of casual graphical analysis that we use. It thus appears likely that the number of exponential terms we find in the capacitive transient reflects the precision of our data and our curve-fitting process, and does not define a number of discrete steps in which the preparation's membrane capacitance is actually discharged. In this interpretation, the values of r_{s2}, r_{s1}, r_{s0}, C_{m2}, C_{m1}, and C_{m0} are a lumped representation of how capacitance and resistance to radial current flow are distributed throughout that portion of our preparation which is in the test node.

At this stage in the construction of our equivalent circuit we insert ion conductance channels in parallel with the capacitance elements. In our experiments we applied TEA to eliminate any slowly rising K^+ current, so we do not include such channels in the model either. We do insert a leakage conductance with an absolute reversal potential of -70 mV and a magnitude of 0.1 mmho/cm². This degree of leak has only a small effect on the simulated voltage clamp currents. For the time being we omit a possible calcium, or slower inward transient and insert almost-standard Hodgkin-Huxley sodium channels (Palti, 1973) as a first attempt at simulating the rapid inward transient current. In our channels, the standard values of α_m, β_m, α_h, β_h, and E_{Na} are retained, but the value of $\bar{g}_{Na}$ is set empirically to give the best fit to the magnitude of the experimentally determined fast inward transient. For the preparations we simulated, the best fits were given by values of $\bar{g}_{Na}$ in the range of 30–40 mmho/cm² (one-quarter to one-third of the standard squid axon channel density).

The full equivalent circuit for the preparation, including ion channels, is shown in Fig. 2. If the potential between the bathing solution and cell interiors is clamped at a value of V_c then the time courses of the membrane potentials V_{m2}, V_{m1}, V_{m0} (across the capacitors C_{m2}, C_{m1}, C_{m0}) are given by the equations:

$$dV_{m2}/dt = \{I_{m2} + [(V_c - V_{m2})/r_{s2}] + [(V_{m1} - V_{m2})/r_{s1}]\}/C_{m2}, \qquad (8)$$

$$dV_{m1}/dt = \{I_{m1} + [(V_{m2} - V_{m1})/r_{s1}] + [(V_{m0} - V_{m1})/r_{s0}]\}/C_{m1}, \qquad (9)$$

$$dV_{m0}/dt = \{I_{m0} + [(V_{m1} - V_{m0})/r_{s0}]\}/C_{m0}, \qquad (10)$$

where I_{m2}, I_{m1}, I_{m0} are the ion currents (leakage and sodium) through the individual membrane patches in the model. The simulated *measured* membrane current (as opposed to the simulated *actual* ion currents) is given by:

$$I = (V_{m2} - V_c)/r_{s2}. \qquad (11)$$

The expressions $(V_{m1} - V_{m2})/r_{s1}$ and $(V_{m1} - V_{m0})/r_{s0}$ give current flows through r_{s1} and r_{s0}, respectively.

Some comments are in order on the form and meaning of these equations before proceeding to display the numerical results. First, we should point out that these equations, with V_c = constant, simulate a situation in which we have an absolutely perfect and flat voltage trace during our clamp experiments. In fact, our experimental voltage trace has a rise time of 50–75 μs and is quite flat thereafter, so this assumption of apparently perfect voltage control is reasonably good. Next, Eq. 11 states that the measured membrane current is a direct and simple function of the voltage of the outer layer of cells only. The inner cells contribute only as they affect the membrane potential of the outer cells. Finally, Eq. 11 implies an upper limit or saturation value to the possible measured ionic current no matter what the density of conductance channels. The sodium current, for example, as it is turned on will tend to drive V_{m2} toward V_{Na}. The maximum possible contribution then of the sodium current to the total measured current at any clamp voltage V_c is given by:

$$I_{Na,max} = (V_{Na} - V_c)/r_{s2}. \qquad (12)$$

Fig. 3a shows numerical computations with our full model (Eqs. 8–11) which exemplify this point. The peak inward simulated current is shown as a function of $\bar{g}_{Na}$, and it asymptotes towards $I_{Na,max}$. We might point out that such a saturation phenomenon should theoretically exist for any voltage-clamped tissue, including axons, in which there is extramembrane resistance.in the current injection pathway. The difference between cardiac muscle and axons in this regard is that the value of series resistance is much lower for axons, so that the measuring process is far less distorted by this effect. It can be seen from Fig. 3a that for normal physiological current densities, our cardiac preparation is in a region of the curve of I vs. $\bar{g}_{Na}$ where the current is not directly proportional to $\bar{g}_{Na}$. Also, by noting $V_{m2} - V_c = I/r_{s2}$, one can see that V_{m2} is quite far from the nominal clamp potential during the fast inward current. One might think to get a better look at the sodium current kinetics by reducing $\bar{g}_{Na}$ with application of a small dose of TTX, so that the preparation would function far below $I_{Na,max}$ in the region where $V_{m2} - V_c$ is small. Unfortunately the results shown in Fig. 3b suggest
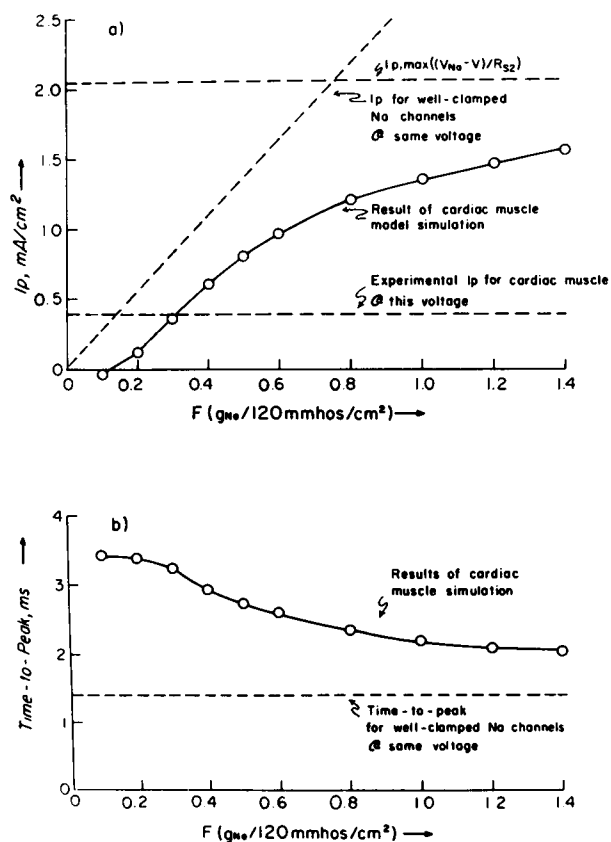
FIGURE 3 Dependence of behavior of rapid inward transient current on sodium channel density ($\bar{g}_{Na}$), showing that in the model the simulated magnitude of the peak inward current is not directly proportional to $\bar{g}_{Na}$ and the kinetics of the inward current are a function of $\bar{g}_{Na}$, in contrast to a preparation for which good trans-membrane voltage control can be assumed. (a) Variation of simulated peak I_{Na} at one voltage vs. $\bar{g}_{Na}$ for frog atrial trabeculae and for well-controlled membrane with same number of sodium channels. Simulated current asymptotes towards $I_{Na,max}$ (Eq. 12 in text) while current of well-controlled preparation climbs linearly with increasing $\bar{g}_{Na}$. (b) Variation of time-to-peak vs. $\bar{g}_{Na}$ for same simulations as 3 a. Resistance-capacitive distribution is derived from capacitive transients of prep. no. 6273, 100 μm node width. Depolarization step to $E = -33$ mV from resting E of -66 mV. F is defined as ratio of $\bar{g}_{Na}$ to value for standard squid axon.

that this cannot be done. In this graph, time-to-peak of rapid inward transient vs. $\bar{g}_{Na}$ is plotted for the same computations as Fig. 3 a. We see that for smaller sodium currents the apparent kinetics of the fast inward current are *farther* from the true kinetics of the Hodgkin-Huxley sodium channels than for the large currents. This is true for a wide range of depolarizing steps, and appears to be because the turning on of the sodium current helps bring the membrane potentials up to the clamp potential faster. It may be noted that for small values of $\bar{g}_{Na}$ at the voltage simulated in Fig. 3 a, the simulated preparation does not even generate a net inward current although there is a

transient *relative* inward peak. Such a phenomenon in an axon preparation could be due to a large leakage current, but that is not true of our cardiac muscle preparation. Here, this phenomenon appears because of the long latency before membranes deep in the preparation depolarize in response to an applied clamp, and the fact that during this latency the extracellular current flow between these deep membranes and the surface membranes is such as to retard the depolarization of the surface cells.

It thus appears that the large resistances in extracellular current pathways in the preparation leave us no "window" through which to see voltage-clamped sodium cur-
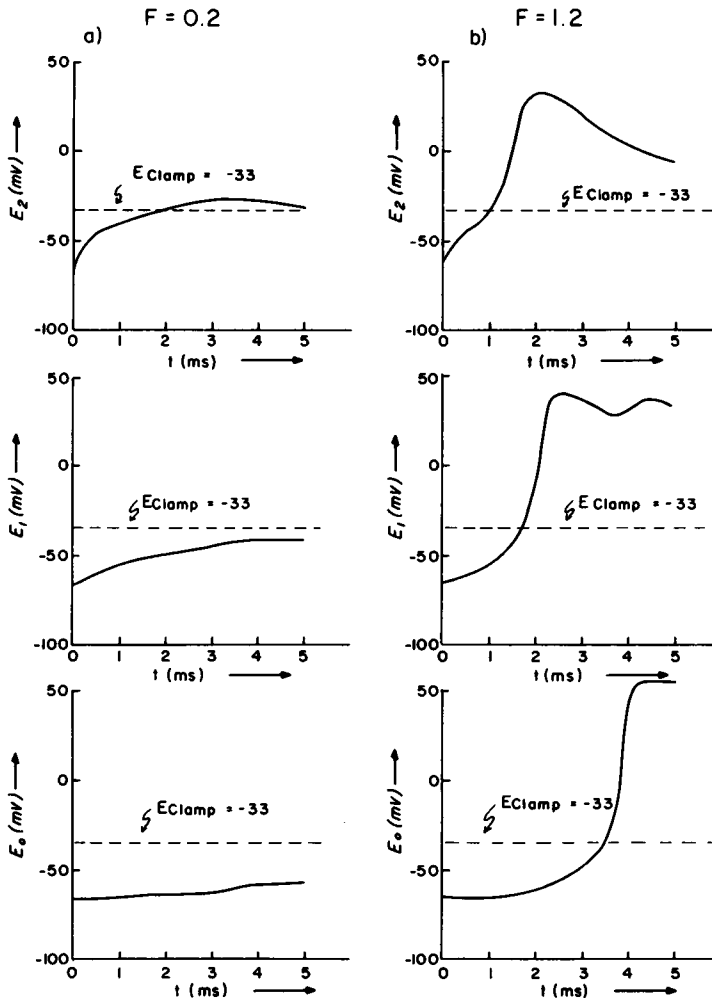

FIGURE 4 Simulated time course of membrane potential in outer, middle, and inner segments of the preparation for large and small $\bar{g}_{Na}$. Calculated by simultaneous numerical integration of Eqs. 8, 9, and 10, respectively, coupled with Hodgkin-Huxley equations for ionic current in each patch. E_2, E_1, E_0 are membrane potential for outer, middle, and inner patches, respectively. $F \equiv \bar{g}_{Na}/(120 \text{ mmho/cm}^2)$.

rents. At physiological sodium current densities the membrane potentials far over-shoot the clamp potential; at lower current densities the overshoot is not so bad but the time lag before the membrane potentials reach the clamp potential is increased. Fig. 4 shows the time course of potential in the model's three patches for a large and a small value of $\bar{g}_{Na}$, demonstrating these points. The first millisecond in 4a, before the sodium current turns on very much, shows something of the passive response. The outer patch relaxes first, followed more slowly by the middle and finally the inner patch.

Fig. 3 gives a prediction of the effects of TTX on this preparation. In addition to reducing the magnitude of the inward transient, just as it would for a preparation with good membrane voltage control, the model also predicts that the apparent inward transient will be made slower by TTX. This agrees with our experimental results, but not with the tentative conclusion that the slower kinetics represent a closer approach to the true membrane kinetics (Connor et al., 1975). Another prediction of the model, exemplified by Fig. 5, is that application of TTX will shift the peak I-V curve along the voltage axis. Experimental results presented in our previous paper (Connor et al., 1975) also show such a shift. The direction and size of the shift vary from preparation to preparation, so it is apparently a complicated effect which is a function of the precise resistance-capacitance distribution of a particular trabecula.

In the voltage clamp simulations described above, and in the others in this paper, the experimental clamps were from rest potential. It is well known (Julian et al., 1962) that preparations in the double sucrose gap become hyperpolarized from normal resting
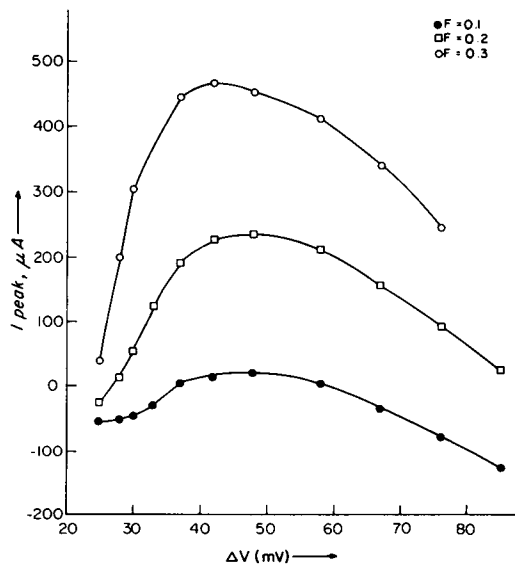

FIGURE 5 Computed shift of model I-V curve along voltage axis with change in $\bar{g}_{Na}$, correspond-ing to same effect observed experimentally with partially-blocking dose of TTX. Parameters derived from capacitive transient of prep. no. 6273, node width 100 μm.
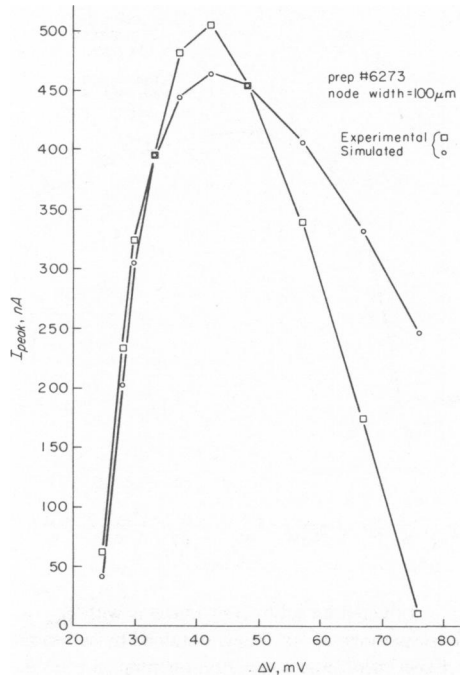$F \equiv \bar{g}_{Na}/(120 \text{ mmho/cm}^2)$.

FIGURE 6 Model uncorrected I-V curve compared with experimental uncorrected I-V curve for same preparation. Prep. no. 6273, node width 100 μm. Resting potential in sucrose gap calculated at -66 mV. $\bar{g}_{Na}/(120\,\mathrm{mmho/cm^2}) = 0.31$.

potential but the absolute amount of this hyperpolarization is variable among preparations. To estimate this for purposes of our simulation of a particular preparation, we set the simulated rest potential at a value which makes the simulated voltage at which the uncorrected peak I vs. V curve is a maximum match the corresponding experimental voltage. The resting potential obtained from this process is always somewhat hyperpolarized from the normal squid axon resting potential of -60 mV. The amount of hyperpolarization varies among preparations, ranging from less than 10 to over 30 mV. Given this adjustment, the uncorrected I-V curve for the model is fairly close to that for the preparation. A comparison for one case is shown in Fig. 6.

A distinct difference appears between the cardiac muscle and typical axonal preparations if we try to measure the rapid inward transient really properly, i.e. by doing a point-by-point subtraction of a current trace in TTX-poisoned Ringer's from a trace at the same clamp voltage in normal Ringer's. Under this procedure, the positive-resistance limb of the corrected I-V curve for both the model and the preparation becomes very flat, projecting a reversal potential which seems unreasonably large for the preparation and which we know is far beyond the reversal potential of the sodium channels in the model. This phenomenon is shown in Fig. 7. The underlying mechanism seems clear from examining the potentials and membrane currents for the individual membrane patches in the model (Fig. 8). In this figure, showing simulation of a
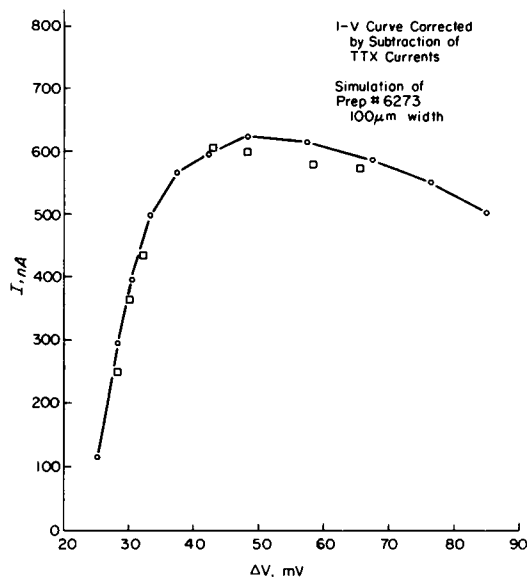
FIGURE 7 Model I-V curve corrected by subtracting currents with $\bar{g}_{Na} = 0$ from currents with normal $\bar{g}_{Na}$, compared with experimental I-V points obtained by subtracting TTX-poisoned current from normal current. Experiments and simulation on prep. no. 6273, node width 100 μm. o, simulation; □, experiment.

clamp to a voltage beyond the sodium potential, it is seen that the rise time of the membrane potentials is slow enough that the sodium channels turn on before the potential gets near the sodium potential, so that there is in fact an inward current surge. This surge does not manifest itself in a measured total inward current, since in this case the sodium current can not drive the membrane potential past the clamp potential, but rather in a more rapid approach to the steady-state value of total current than is achieved in the presence of TTX. Indeed, if one clamps to the sodium reversal potential, the sodium current acts just like a partial feedback compensation for the extracellular series resistance.

Another way in which the model matches the data from the preparation quite closely is in the time-to-peak of the measured inward transient current. Comparison of experimental and simulated time-to-peak for one preparation is shown in Fig. 9. These data tend to support the hypothesis that the preparation sodium channel kinetics at 15°C are about as fast as the H-H channels at 6°C and that the apparent comparative slowness of the fast inward current is due to lags from the resistance-capacitance distribution in the preparation.

It might be noted that we found the model's ability to fit very well the data of Figs. 7 and 9 to be critically dependent on the existence of the long time constant (about 10 ms) component of the capacitive transient and the corresponding existence of the third capacitive patch, deep within the membrane. The reader may have noticed from the capacitive transient data of our previous paper (Connor et al., 1975) that one would
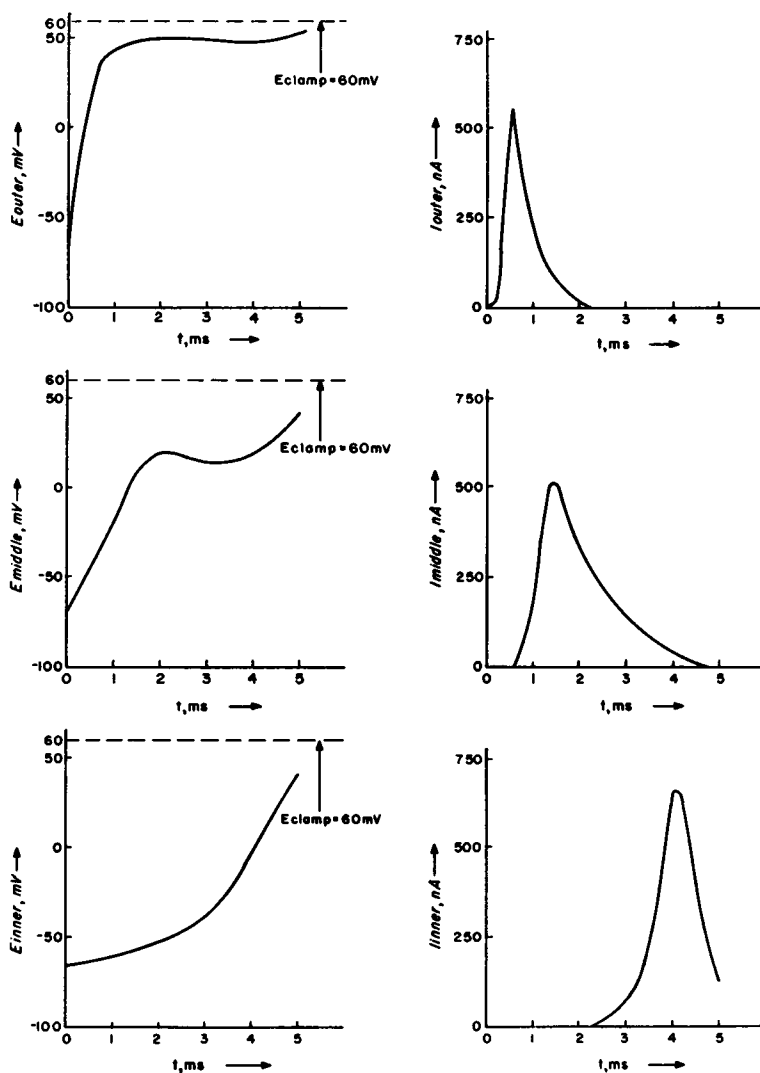
FIGURE 8 Simulated distribution of membrane potential and ionic current for voltage clamp to a level beyond sodium reversal potential. Calculated by simultaneous numerical integration of Eqs. 8, 9, and 10 coupled with Hodgkin-Huxley equations for ionic current in each patch. In simulation, $E_{clamp} = 60$ mV, $E_{Na} = 55$ mV. Resistance-capacitance distribution from prep. no. 6273, node width 100μm.

not see the third component well at a sweep speed and current sensitivity appropriate for the two faster components. In fact, we went for some time without seeing the slow component at all, and did simulations with two-patch models derived from the faster time constants. These models displayed some slowing of the apparent sodium kinetics from the standard H-H behavior and some flattening of the positive resistance limb of the corrected I-V curve, but both of these effects were small in magnitude compared to
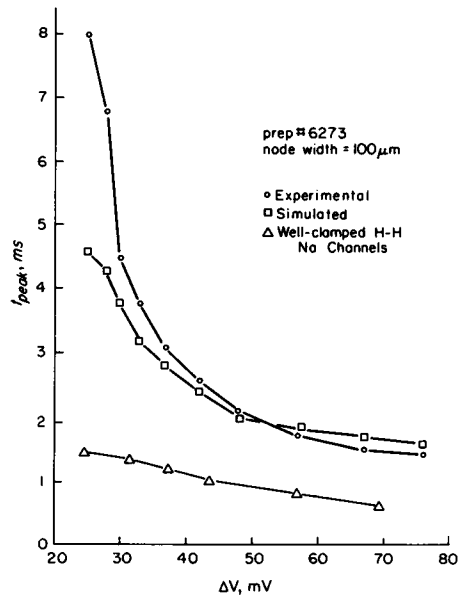
FIGURE 9 Experimental and simulated time-to-peak of rapid inward transient current. Note comparison with time-to-peak of perfectly clamped H-H sodium channels, which are the sodium channels in the simulation. Resistance-capacitance distribution according to capacitive transient of prep. no. 6273, 100 μm node width.

those observed experimentally. It appeared that if we put into the model sodium channels with slower kinetics we could match the time-to-peak data but the corrected *I-V* curves would actually become steeper on the positive resistance limb, thus becoming less like the experimental results. On the other hand, some rough calculations showed that the postulate of a section of membrane deep within the preparation whose capacitance would relax with a primary time constant of several milliseconds might push the model towards a better quantitative fit of both pieces of data simultaneously. This led us to acquire more data on the capacitive transient, this time including observations at slower sweep speeds and higher current sensitivities. The result was that the suspected slow component in the capacitive transient was discovered. We might note that the good fits to the Figs. 7 and 9 data depend mostly on the capacitive properties of the inner patch of membrane and not much on the presence of sodium channels in that patch. Omission of the sodium channels from the inner patch causes only small changes in the time-to-peak and magnitude of the simulated inward transient current. The primary manifestation of the inner patch sodium current in the simulated total current is as secondary peaks or notches, which also sometimes occur in the experimental data.

The model presented in this paper has two major defects in simulating the experimental current traces. One is that the secondary peaks in the model, although coming with about the correct delay, are larger than the corresponding features in the experimental data. The second is that the decay time of the primary peak of the measured
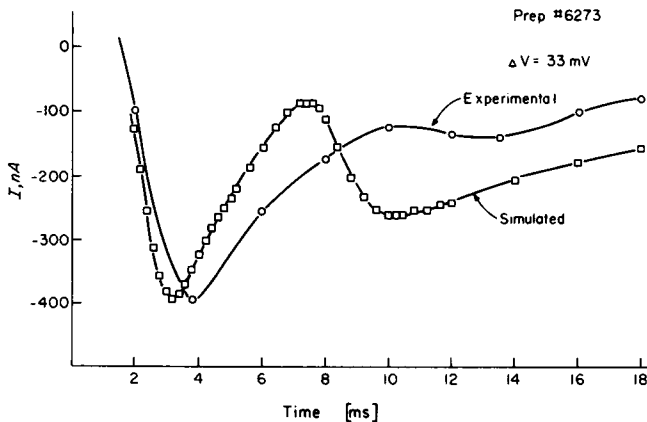
FIGURE 10 Experimental and simulated current trace from same preparation, showing discrepancies in inactivation rate of first peak and size of secondary peak.

inward transient is more rapid in the simulated than in the experimental current traces. These points are illustrated in Fig. 10, in which an experimental and a simulated current trace for the same preparation undergoing the same voltage step are superimposed on each other. The identification of the secondary peak with the surge of inward ionic current in the inner membrane patch is clear from Fig. 11, which shows the voltages and ionic currents for each patch for the same computation as Fig. 10.

There are a number of possible refinements of the model which may help it overcome its remaining deficiencies without, hopefully, sacrificing any of its successful features. With regard to the size of the secondary total peak, this could be made smaller to any desired extent without significantly affecting the first peak by reducing $\bar{g}_{Na}$ and V_{Na} for the inner cells. There is physical reasonableness to this modification if one postulates some mixing between the saline and sucrose solutions within the preparation, so that inner cells in the "test node" (how does one define the "test node" if one postulates sucrose-saline mixing?) are exposed to lower sodium concentration than are surface cells. As far as the too-rapid falling off of the simulated first peak, one should at least consider the possibility that the slow experimental decay time of this peak is because inactivation of sodium channels in cardiac muscle is actually slower than in other excitable membranes. The effects of these and other reasonable modifications to the model should be examined carefully. Included in these other modifications should certainly be possible refinements of the equivalent circuit, such as representing the radial distribution of capacitance by more than three capacitive elements, which is equivalent to using a finer grid for numerical integration in the radial direction in space; and introducing a consideration of nonhomogeneity along the *length* of that portion of the preparation in the test node, which the model does not now consider.

Preliminary computations have been done with five and seven capacitive elements representing radially distributed capacitance and they do in fact show a slowing of the falling off of the first peak and a reduction in magnitude of the second peak. This work is continuing.
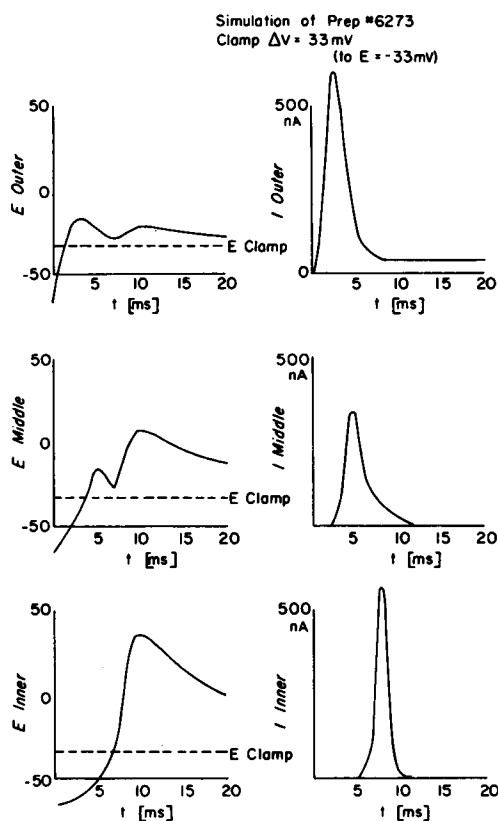
FIGURE 11 Distributed membrane voltage and ionic current for same simulation as Fig. 10.

SUMMARY

An equivalent circuit was derived for frog atrial muscle in the double sucrose gap. To do this, a reasonably simple distribution of extramembrane resistance and membrane capacitance was deduced from the form of the preparation's capacitive decay, and near-standard Hodgkin-Huxley ion conductance channels were inserted in parallel with the simulated membrane capacitance. The resulting circuit gives good simulations for a variety of ways in which the cardiac muscle rapid inward transient current differs from that in well-clamped axons. These include time-to-peak, the flattening effect on the I-V curve of correcting for capacitive transient by subtracting TTX-poisoned current traces, and the slowing of time-to-peak by partial poisoning with TTX. Both the preparation and the simulation currents shift along the voltage axis of the I-V curve on partial poisoning with TTX. Ways in which the equivalent circuit behaves differently from the preparation are exaggerated secondary peaks and notches and too-rapid decay of the primary inward transient. Possible reasons for these discrepancies are tentatively suggested.

REFERENCES

ADRIAN, R. H., and L. D. PEACHEY. 1973. Reconstruction of the action potential of frog Sartorius muscle. *J. Physiol.* **235**:103.

BEELER, G. W., and H. REUTER. 1970. Voltage clamp experiments on ventricular myocardial fibers. *J. Physiol.* **207**:165.

COLE, K. S. 1968. Membranes, Ions, and Impulses. University of California Press, Berkeley. 373–417.

CONNOR, J., L. BARR, and E. JAKOBSSON. 1975. Electrical characteristics of frog atrial trabeculae in the double sucrose gap. *Biophys. J.* **15**:1047.

EIGEN, M., and L. DEMAEYER. 1963. Relaxation methods. *In* Techniques of Organic Chemistry. Vol. VIII, Pt. 2. S. L. Fliess, E. S. Lewis, and A. Weissberger, editor. 895–1054, Interscience, New York.

HELLAM, D. C., and J. W. STUDT. 1974 *a*. A core-conductor model of the cardiac Purkinje fibre based on structural analysis. *J. Physiol.* **243**:637.

HELLAM, D. C., and J. W. STUDT. 1974 *b*. Linear analysis of membrane conductance and capacitance in cardiac Purkinje fibers. *J. Physiol.* **243**:661.

HODGKIN, A. L., and A. F. HUXLEY. 1952 *a*. Currents carried by sodium and potassium ions through the membrane of the giant axon of *Loligo*. *J. Physiol.* **116**:449.

HODGKIN, A. L., and A. F. HUXLEY. 1952 *b*. The components of membrane conductance in the giant axon of *Loligo*. *J. Physiol.* **116**:473.

HODGKIN, A. L., and A. F. HUXLEY. 1952 *c*. The dual affect of membrane potential on sodium conductance in the giant axon of *Loligo*. *J. Physiol.* **116**:497.

HODGKIN, A. L., and A. F. HUXLEY. 1952 *d*. A quantitative description of membrane current and its application to conduction and excitation in nerve. *J. Physiol.* **117**:500.

JOHNSON, E. A., and M. LIEBERMAN. 1971. Heart: excitation and contraction. *Annu. Rev. Physiol.* **33**:479.

JULIAN, F. J., J. W. MOORE, and D. E. GOLDMAN. 1962. Current-voltage relations in the lobster giant axon membrane under voltage clamp conditions. *J. Gen. Physiol.* **45**:1195.

KOOTSEY, J. M., and E. JOHNSON. 1972. Voltage clamp of cardiac muscle. *Biophys. J.* **12**:1496.

PALTI, Y. 1973. Digital computer solutions of membrane currents in the voltage clamped giant axon. *In* Biophysics and Physiology of Excitable Membranes. W. Adelman, editor. 183–193. Van Nostrand Reinhold, New York.

ROUGIER, O., G. VASSORT, and R. STÄMPFLI. 1968. Voltage clamp experiments on frog atrial heart muscle fibres with the sucrose gap technique. *Pluegers Arch. Gesamte Physiol.* **301**:91.

TARR, M. 1971. Two inward currents in frog atrial muscle. *J. Gen. Physiol.* **58**:523.

TARR, M., and J. W. TRANK. 1974. An assessment of the double sucrose gap voltage clamp technique as applied to frog atrial muscle. *Biophys. J.* **14**:627.